# Supporting Information

## Ion-dipole interaction motivated $Zn^{2+}$ pump and anion repulsion interface enable ultrahigh-rate Zn metal anodes†

Song Huang,[a] Rong Tang,[b] Xiaoqing Liu,[a] Yufei Zhang,[a] Yongchao Tang,[a] Zhipeng Wen, [a] Minghui Ye,[a] Yang Yang,* [b] and Cheng Chao Li*[a]

[a] *Guangdong Provincial Key Laboratory of Plant Resources Biorefinery, School of Chemical Engineering and Light Industry, Guangdong University of Technology, Guangzhou 510006, China. E-mail: licc@gdut.edu.cn*

[b] *College of Chemistry and Chemical Engineering, State-Province Joint Engineering Laboratory of Power, Source Technology for New Energy Vehicle, State Key Laboratory of Physical Chemistry of Solid Surfaces, Xiamen University, Xiamen 361005, P. R. China. E-mail: yangyang419@xmu.edu.cn*

† Electronic Supplementary Information (ESI) available: 10.1039/x0xx00000x

## 1. Experiment Section

***Chemicals:*** $ZnSO_4 \cdot 7H_2O$ (AR), perfluoropentanoic acid (PFPA, >97%) and iodine ($I_2$, >99.8%) were purchased from Aladdin (Shanghai, China). Zn foil (99.95%) and Cu foil (99.95%) were purchased from Zhonghui Keyan. Such chemicals were used as received.

***Preparation of Materials:*** The Zn@PFPA electrode was fabricated by a simple organic acid etching route. Specifically, zinc foils with a thickness of 100 um were sonicated in acetone for ten minutes to wash away surface impurities. The clean zinc flakes were cut into suitable sizes and then immersed in 0.3 M PFPA solution for a duration of 2 hours for in-situ growth and etching. The processed zinc foils were rinsed with water several times and dried naturally to obtain the Zn@PFPA. Subsequently, the Zn@PFPA is cut into 12 mm discs for assembling batteries. The zinc perfluorovalerate powder is fabricated by mixing the PFPA and the ZnO with a molar ratio of 2:1 in the ethanol solvent. The reaction is heated to 40 ℃ under string until the suspended ZnO is completely reacted. Whereafter, the product was cooled down to room temperature, and the solvent was volatilized to obtain white zinc perfluorovalerate (ZP) powder.

***Material Characterizations:*** The XPS spectra were tested by ESCALABMKLL X-ray photoelectron spectroscopy (VG Instruments). The XRD patterns were obtained by X-ray diffractometer (D8 VENTURE, Bruker, Germany). The FT-IR spectra were carried out by FT-IR spectrometer (Nicolet iS5, Thermo Scientific). The contact angle measurements were conducted on the OCA 100 (Dataphysics) contact angle meter.

The SEM images were obtained by field emission scanning electron microscope (SU8220, Hitach, Japan). The in-situ optical images were obtained on a Nikon LV150N microscope by using a homemade in-situ optical electrochemical cell. The in-situ pH test was conducted by the PHB-3 pH meter using the cuvette batteries.

***Electrochemical Measurements:*** For the Zn-$I_2$ full battery, iodine powder and activated carbon were homogeneously mixed in a mass ratio of 1:1 as the active materials. The active materials, carboxymethyl cellulose (CMC) and super P were mixed in an appropriate amount of water in a mass ratio of 8:1:1 to form a slurry, which was then coated on a carbon cloth to prepare the cathode. To fabricate the Cu@PFPA electrode, zinc perfluorovalerate and polyvinylidene fluoride are mixed with a mass ratio of 9:1 in an appropriate amount of N-methylpyrrolidone to form a slurry, followed by coating on the Cu foils. The full batteries were assembled using CR2032 coin-type cells. The loading mass of the iodine cathode is 8.5-9 mg $cm^{-2}$ in coin cells and ca. 6.0 mg $cm^{-2}$ in the pouch cells. The rate and long-term cycling performance of Zn-$I_2$ batteries were conducted by galvanostatic discharge/charge (GDC) tests with a voltage range of 0.6-1.6 V. The symmetric and half batteries were also performed by GDC tests and the cut-off capacity was set as 1 mAh. The charging cutoff voltage for a half cell is 0.5 V. The zinc foils/Zn@PFPA and the Whatman GF/D glass microfibers papers were served as the anode and separators, respectively. The 2 M $ZnSO_4$ was employed as an electrolyte for both symmetric, asymmetric and full batteries. The GDC tests were performed on a Neware battery testing system (CT-4008-5V6A, Shenzhen, China). The cyclic voltammetry (CV), Chronoamperometry

(CA) and Linear sweep voltammetry (LSV) curves were obtained on a Gamry electrochemical workstation with a three-electrode system (Zn foil as work electrode, Pt as counter electrode, and Ag/AgCl as reference electrode). Electrochemical impedance spectroscopy (EIS) in a two-electrode system was scanned with the frequency range from 100 kHz to 0.01 Hz. Zn||Cu and Zn||Zn cells were assembled to evaluate the CE and cycling life using CR2032 coin-type cells.

***Theoretical calculations:*** Quantum chemistry (QC) calculation was performed with Gaussian09 E.01[1] software in this work. The B3LYP-D3[2,3] functional was used as it is robust for elements and helpful in improving the precision of weak interactions. 6-311+G(d,p)[4-8] basis set was used for C, H, O and F atoms while Lanl2TZ[9,10] basis set was used for Zn atoms. Molecules were optimized and had no imaginary frequency in vibration analysis. In the adsorption energy ($E_{ads}$) calculation, the two segments are optimized, respectively. Solvent effects of water ($\varepsilon$ = 78.4) were considered by SMD[11]solvation model. The electrostatic potential (ESP) and restrained electrostatic potential (RESP)[12] were calculated through Multiwfn[13,14] software. The adsorption energy of the $Zn^{2+}$ was defined as:

$$E_{ads} = E_{Zn2+/surf} - E_{surf} - E_{Zn2+}(g)$$

where $E_{Zn2+/surf}$, $E_{surf}$ and $E_{Zn2+}(g)$ correspond to the energy of adsorbate $Zn^{2+}$ adsorbed on the surface, the energy of the surface, and the energy of $Zn^{2+}$, respectively.

The B3LYP-D3[2,3] functional and def2-SVP[15] basis set was used to optimize the geometry of all structures. The vibration analysis was performed at the same

theoretical level to ensure that all structures are energy minima and get Gibbs-free energy correction. The high-precision single-point energy was calculated by Gaussian09 E.01 at the B3LYP-D3/def2-TZVPP[15,16] theoretical level. Solvent effects of water was considered by SMD[11] solvation model at M05-2X[17]/6-31G(d)[18-21].The desolvation energy is defined as:

$E=E(i\text{-}nH_2O)-E(i)-nE(H_2O)$

Where E is the desolvation energy of $[Zn(H_2O)_6]^{2+}$ (or Zn-2PFPA-$nH_2O$)，E(i-$nH_2O$) is the energy of $[Zn(H_2O)_6]^{2+}$ (or Zn-2PFPA-$nH_2O$), E(i) is the energy of $Zn^{2+}$ (or Zn-2PFPA), and E($H_2O$) is the energy of $H_2O$.

Molecular dynamics (MD) simulation was performed through Gromacs2018.8[22] software to study the Zn/electrolyte interface structure at different potentials. The small molecules (PFPA, water, $ZnSO_4$) were reasonably optimized via Gaussian09 E.01[1] software with a level of B3LYP-D3[2,3] functional and def2-SVP[15] basis set before simulations. The force field parameters of $Zn^{2+}$ ions and SPC/E[23] water model was obtained with Amber99SB[24] force field. The GAFF[25] force field parameters of sulfate ion were generated with Acpype program[26] , PFPA was generated with Sobtop software[27]. Leonard-Jones parameters of metal zinc atoms were set as $\sigma$ = 2.44 Å and $\varepsilon$ = 3.022 kJ $mol^{-1}$, which shows good accuracy in the interface. RESP atom charges were used to describe electrostatic interactions. Atomic charges of all ions were multiplied by scale factor 0.7 to correct the polarization effect of ions. A constraint potential (force constant = $1 \times 10^5$ kJ $mol^{-1}$) in the x, y and z axes for Zn atoms in the electrode was used to maintain the structure of

metallic zinc. The electrode potential was controlled with the charge density of the zinc metal surface. Zero-charge potential (PZC) was used to approximate the equilibrium potential of $Zn/Zn^{2+}$ in aqueous phase as they are similar.[28] The interface capacitance was set to 40 μF $cm^{-1}$ .[29]

The composition of the simulation box is 2M $ZnSO_4$ +PFPA, including 2508 Zn atoms, 150 PFPA, 120 $ZnSO_4$ and 2833 $H_2O$. An 6-layer slab containing 2508 Zn atoms was built in Material studio[30][31], which used as the model of [0 0 1] surface of the Zn electrode. The boxes of $ZnSO_4$ aqueous solution were built by filling molecules randomly. The initial structures were modelled via Packing Optimization for Molecular Dynamics Simulations (Packmol) program[32] and the periodic box was set to 10*10*10 $nm^3$. For zinc PFPA covered surface, 150 PFPA, 75 $Zn^{2+}$ ions and 500 $H_2O$ molecules were spread on the electrode surface. After 20 ns NPT pre-equilibration at 298.2 K and 100 bar, other $Zn^{2+}$ ions, $SO_4^{2-}$ ions and $H_2O$ were filled into the box. All the boxes were first submitted to energy minimization by using the 10000-step steepest descent method in order to avoid unreasonable contact of system. At this time, the size of simulation is 51.10 Å, 51.24 Å and 63.98 Å in the x, y, z axes. The equilibrium simulation was carried out with NPT ensemble at 298.2 K and 1 bar for 20 ns, the non-bonding cutoff radius was 1 nm and the integration step was 1 fs. The production simulation was carried out with NVT ensemble at 298.2 K for 20 ns. The RDF function and distribution of number density was calculated through Gromacs2018.8. VMD[33] software was used to visualize the systems and obtain the ion association state. Only the final 5 ns was sampled for radial distribution function

(RDF) and coordination structure counting analyses. A time step of 1 fs was used for all simulations.

## 2. Figures and tables

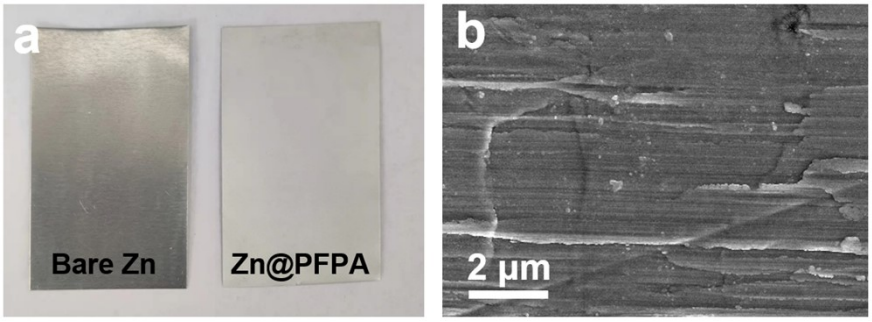


**Figure S1.** (a) Comparison of surfaces before and after PFPA treatment. (b) The bare zinc surface exhibits visible bumps due to machining.

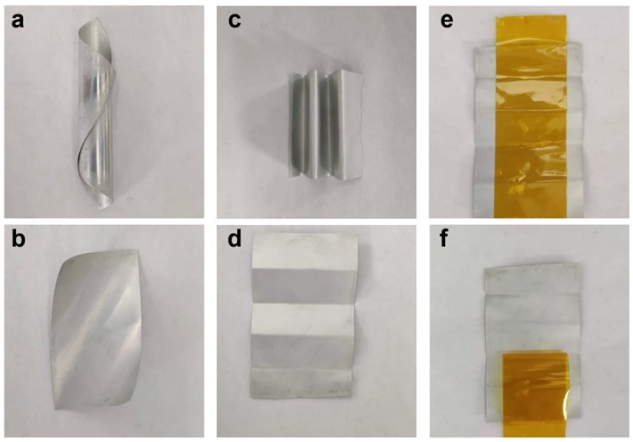


**Figure S2.** The toughness test of Zn@PFPA with curling (a, b), folding (c, d) and tearing with adhesive tape (e, f).

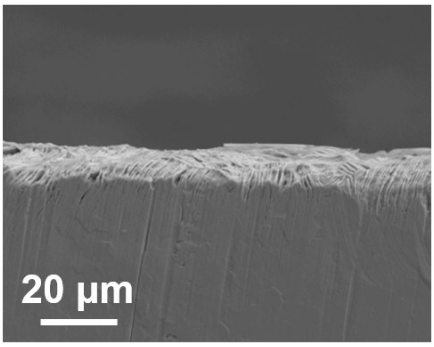


**Figure S3.** The cross-sectional SEM images of Zn@PFPA after acid etching.

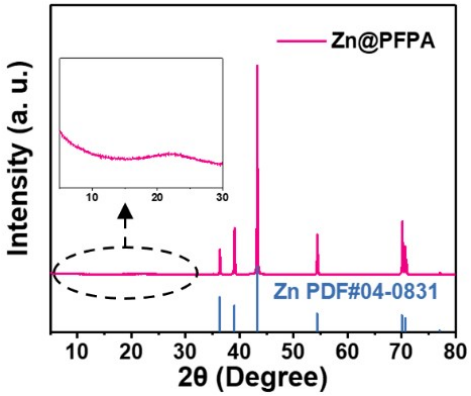


**Figure S4.** The XRD pattern of the Zn@PFPA electrode.

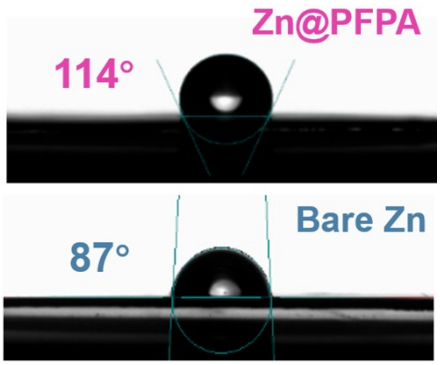


**Figure S5.** The contact angle test of the bare Zn and Zn@PFPA.

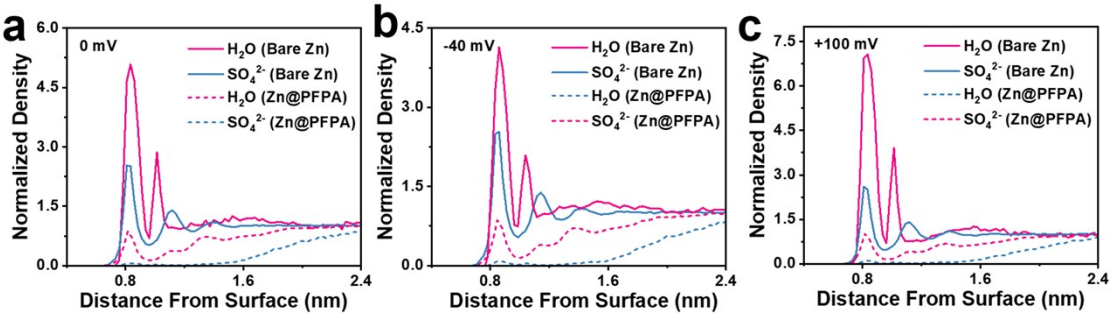


**Figure S6.** The normalized density of $H_2O$ molecules and $SO_4^{2-}$ with bare Zn and Zn@PFPA interface at different biases obtained by MD simulation.

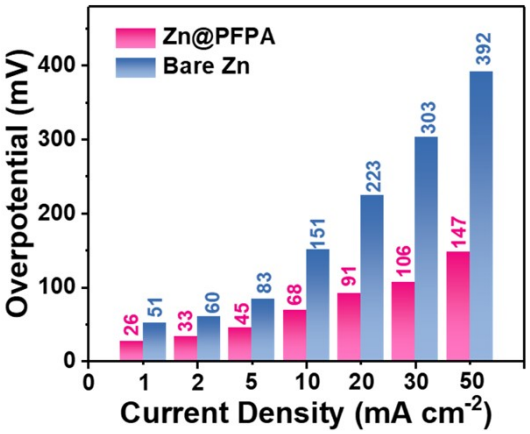


**Figure S7.** The polarization potential of bare Zn and Zn@PFPA at different current density.

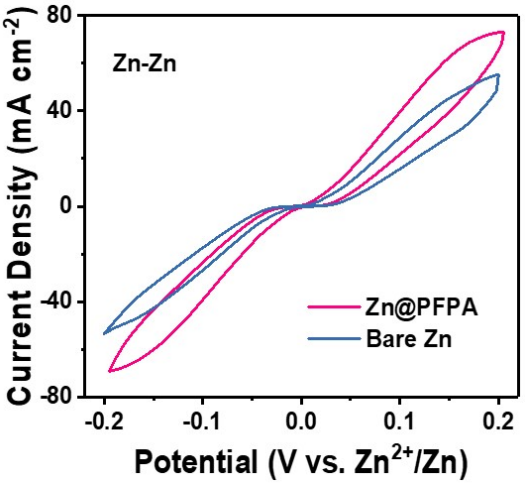


**Figure S8.** The CV curves of symmetric batteries.

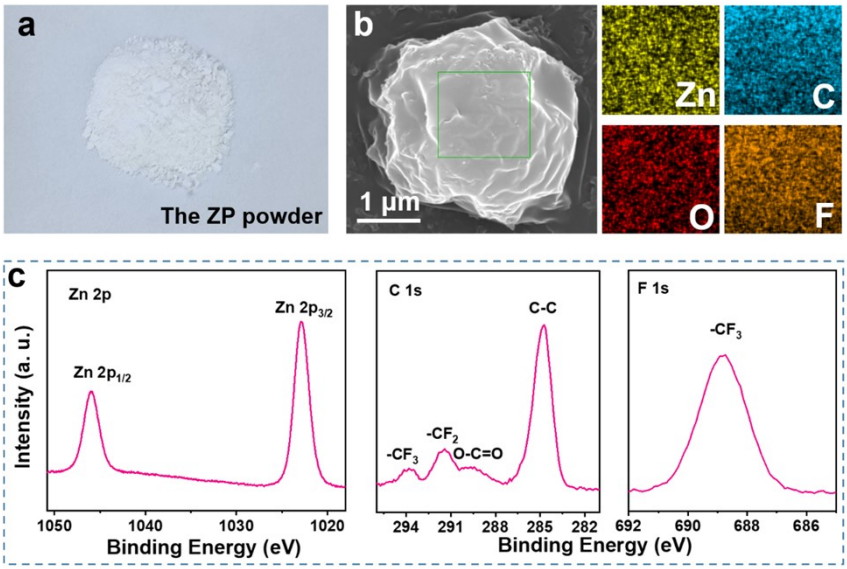


**Figure S9.** (a) The digital photo of the as-fabricated zinc perfluorovalerate (ZP) powder. (b) The SEM images and corresponding element mapping of the ZP. (c) The high-resolution XPS spectra of the ZP. The Zn, O, F and C elements are uniformly distributed in the as-prepared ZP, confirming the successful synthesis. Additionally, the high-resolution XPS spectra identify also the formation of the ZP.

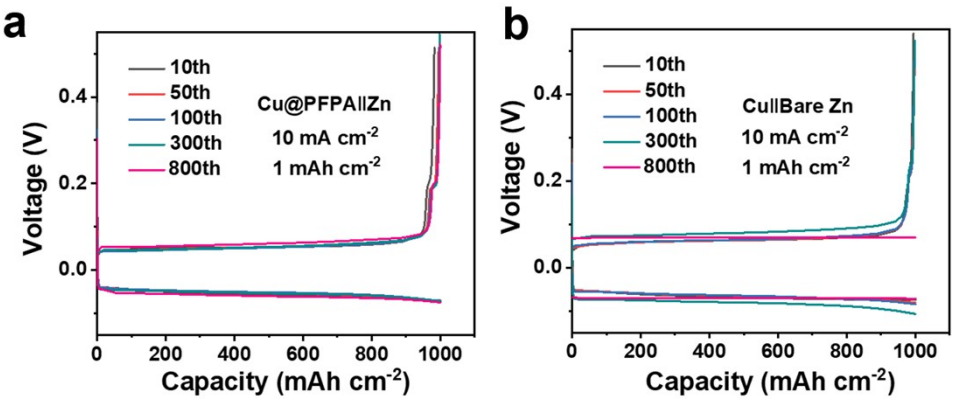


**Figure S10.** (a, b) The asymmetric batteries of bare Zn and Zn@PFPA at 10 mA $cm^{-2}$ in different cycles.

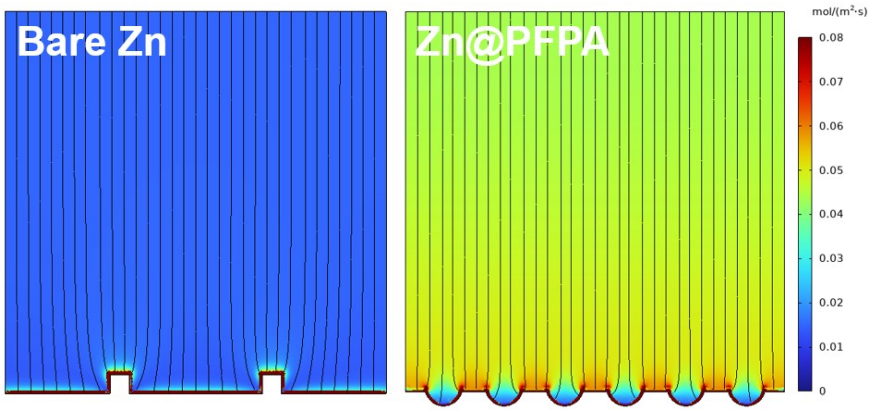


**Figure S11.** The COMSOL simulation of Zn ion concentration distribution for bare Zn and Zn@PFPA elecreode.

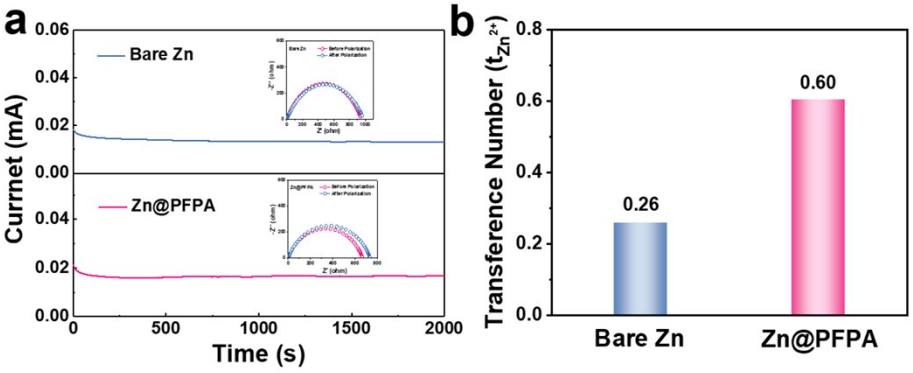


**Figure S12.** (a) The chronoamperometry (CA) curves and corresponding EIS plots. (b) The $Zn^{2+}$ transference number for the bare Zn and Zn@PFPA electrodes.

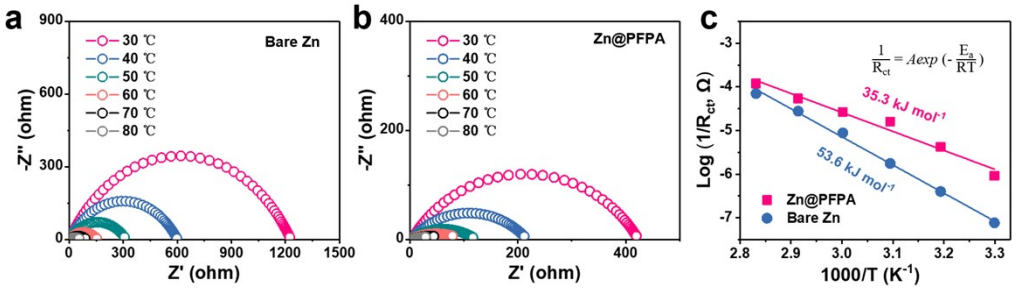


**Figure S13.** (a, b) The impendence at different temperature for bare Zn and Zn@PFPA electrodes. (c) The desolvation activation energy of bare Zn and Zn@PFPA electrodes.

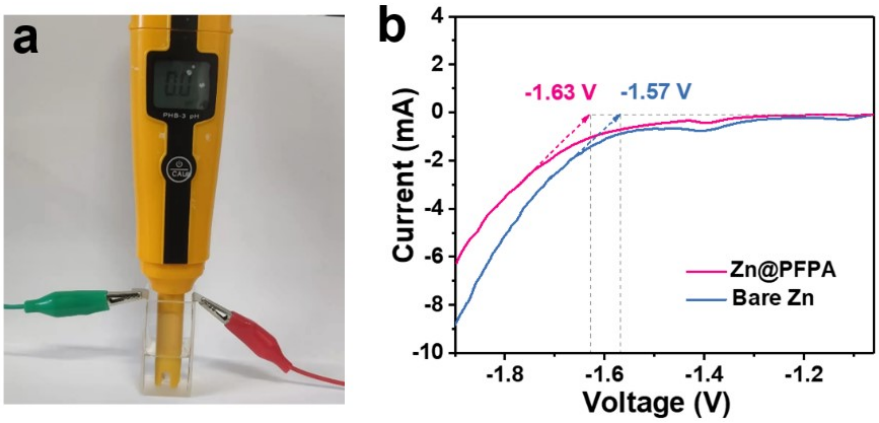


- **Figure S14.** (a) The pH measuring device consisted of a pH-meter and cupola battery. (b) HER curves in the electrolyte of 1M $Na_2SO_4$.

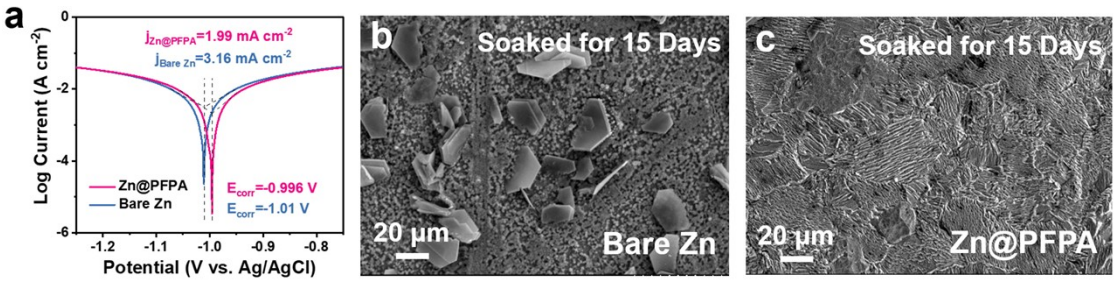


**Figure S15.** (a) The Tafel curves for bare Zn and Zn@PFPA electrodes. (b, c) The surficial morphology of bare Zn (b) and Zn@PFPA (c) electrodes after soaking for 15 days with 2M $ZnSO_4$.

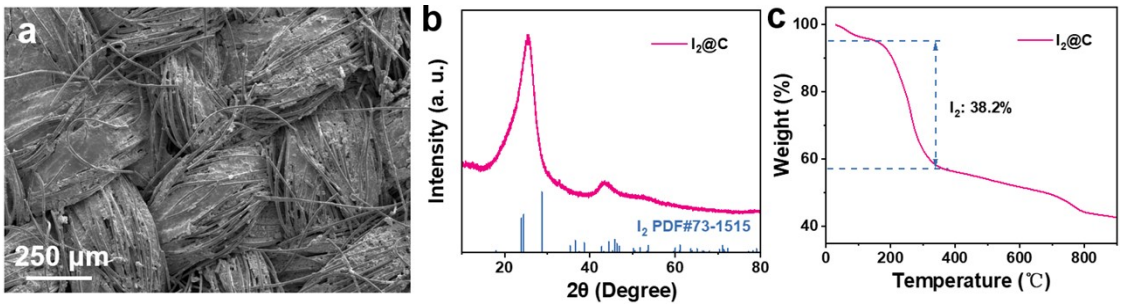


**Figure S16.** The corresponding characterizations of the $I_2$@C cathode. (a) The SEM image of the $I_2$@C coated on the carbon cloth. (b) The XRD pattern. (c) The thermogravimetric (TG) analysis.

**Notes:** the typical iodine diffraction peak is not detected in the XRD pattern of the $I_2$@C cathode, indicating the $I_2$ was adequately dispersed in the active carbon. The TG analysis suggests that the content of $I_2$ in the $I_2$@C is ca. 38.2 wt%.

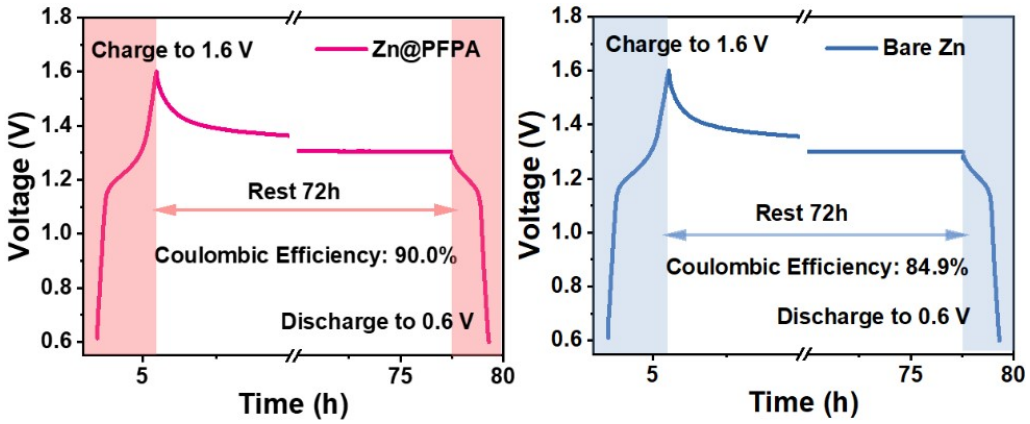


**Figure S17.** The self-discharging test of Zn-$I_2$ batteries for the Zn@PFPA and bare Zn electrodes.

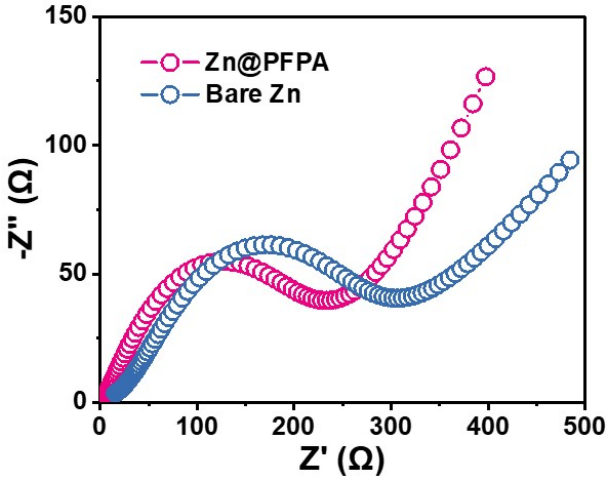


**Figure S18.** The impedance plots of Zn-$I_2$ batteries for the Zn@PFPA and bare Zn electrodes.

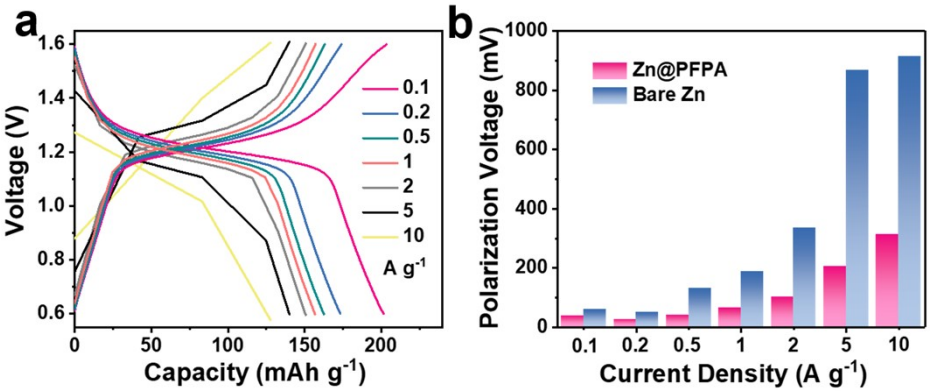


**Figure S19.** (a) The Voltage profiles in different current densities of Zn@PFPA-$I_2$ battery. (b) The comparison of polarization voltage for bare Zn and Zn@PFPA

electrodes in various current densities.

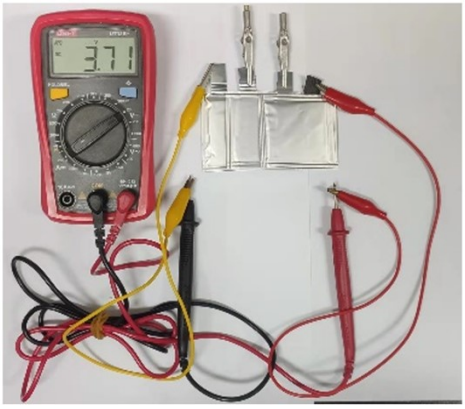


**Figure S20.** Three pouch batteries in series afford a voltage of 3.71 V.

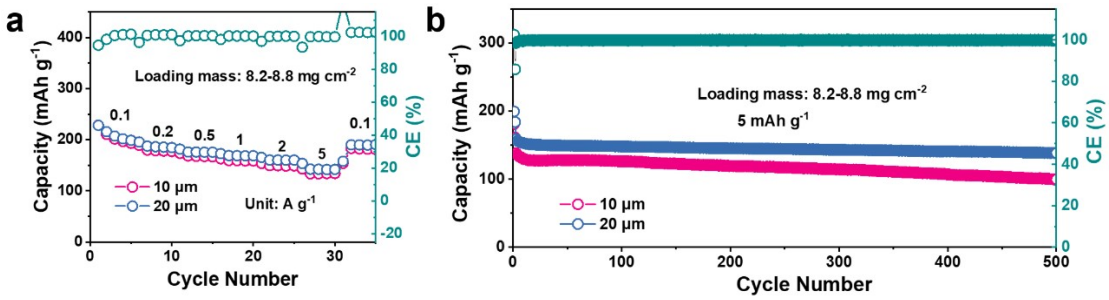


**Figure S21.** (a, b) The rate (a) and cycling (b) performance of Zn-$I_2$ batteries with thin Zn@PFPA electrode (10 and 20 μm).

**Reference**


1. Frisch, M. J.; Trucks, G. W.; Schlegel, H. B.; Scuseria, G. E.; Robb, M. A.; Cheeseman, J. R.; Scalmani, G.; Barone, V.; Mennucci, B.; Petersson, G. A.; et al. *Gaussian 09, Revision E.01*; Gaussian, Inc., Wallingford CT, 2013.
2. Stephens, P. J.; Devlin, F. J.; Chabalowski, C. F.; Frisch, M. J. Ab Initio Calculation of Vibrational Absorption and Circular Dichroism Spectra Using Density Functional Force Fields. *J. Phys. Chem.* 1994, *98* (45), 11624-11627.
3. Grimme, S.; Antony, J.; Ehrlich, S.; Krieg, H. A consistent and accurate ab initio parametrization of density functional dispersion correction (DFT-D) for the 94 elements H-Pu. *J. Chem. Phys.* 2010, *132* (15), 154104.
4. G. W. Spitznagel, T. Clark, P. von Ragué Schleyer and W. J. Hehre, J. Comput. Chem., 1987, 8, 1109.
5. T. Clark, J. Chandrasekhar, G. W. Spitznagel and P. V. R. Schleyer, J. Comput. Chem., 1983, 4, 294.
6. M. M. Francl, W. J. Pietro, W. J. Hehre, J. S. Binkley, M. S. Gordon, D. J. DeFrees and J. A. Pople, J. Chem. Phys., 1982, 77, 3654.
7. A. D. McLean and G. S. Chandler, J. Chem. Phys., 1980, 72, 5639.
8. R. Krishnan, J. S. Binkley, R. Seeger and J. A. Pople, J. Chem. Phys., 1980, 72, 650.
9. L. E. Roy, P. J. Hay and R. L. Martin, *J. Chem. Theory Comput.*, 2008, **4**, 1029.
10. P. J. Hay and W. R. Wadt, *J. Chem. Phys.*, 1985, 82, 270.
11. A. V. Marenich, C. J. Cramer and D. G. Truhlar, *J. Phys. Chem. B*, 2009, 113,

6378.

12. P. C. Christopher I. Bayly, and C. Wendy D, 5 and Peter A. Kollman*, J. Phys. Chem., 1993, 97, 10269.
13. T. Lu and F. Chen, *J Comput. Chem.*, 33, 580.
14. J. Zhang and T. Lu, *Phys. Chem. Chem. Phys.*, 2021, 23, 20323.
15. Weigend, F.; Ahlrichs, R. Balanced basis sets of split valence, triple zeta valence and quadruple zeta valence quality for H to Rn: Design and assessment of accuracy. Phys Chem Chem Phys 2005, 7 (18), 3297-3305.
16. Weigend, F. Accurate Coulomb-fitting basis sets for H to Rn. Physical Chemistry Chemical Physics 2006, 8 (9).
17. Zhao, Y.; Schultz, N. E.; Truhlar, D. G. Design of Density Functionals by Combining the Method of Constraint Satisfaction with Parametrization for Thermochemistry, Thermochemical Kinetics, and Noncovalent Interactions. J. Chem. Theory Comput. 2006, 2 (2), 364-382.
18. Hariharan, P. C.; Pople, J. A. The influence of polarization functions on molecular orbital hydrogenation energies. Theor. Chim. Acta 1973, 28 (3), 213-222.
19. Ditchfield, R.; Hehre, W. J.; Pople, J. A. Self-Consistent Molecular-Orbital Methods. IX. An Extended Gaussian-Type Basis for Molecular-Orbital Studies of Organic Molecules. J. Chem. Phys. 1971, 54 (2), 724-728.
20. Hehre, W. J.; Ditchfield, R.; Pople, J. A. Self—Consistent Molecular Orbital Methods. XII. Further Extensions of Gaussian—Type Basis Sets for Use in

Molecular Orbital Studies of Organic Molecules. J. Chem. Phys. 1972, 56 (5), 2257-2261.

21. Rassolov, V. A.; Pople, J. A.; Ratner, M. A.; Windus, T. L. 6-31G* basis set for atoms K through Zn. J. Chem. Phys. 1998, 109 (4), 1223-1229.
22. M. J. Abraham, T. Murtola, R. Schulz, S. Páll, J. C. Smith, B. Hess and E. Lindahl, SoftwareX, 2015, 1-2, 19.
23. H. J. C. Berendsen, J. R. Grigera and T. P. Straatsma, J. Phys. Chem., 1987, 91, 6269.
24. K. Lindorff-Larsen, S. Piana, K. Palmo, P. Maragakis, J. L. Klepeis, R. O. Dror and D. E. Shaw, Proteins: Structure, Function, and Bioinformatics, 2010, 78, 1950.
25. J. Wang, R. M. Wolf, J. W. Caldwell, P. A. Kollman and D. A. Case, J Comput. Chem., 2004, 25, 1157.
26. A. W. S. d. Silva and W. F. Vranken, BMC Research Notes, 2012, 5, 367.
27. Lu, T. Sobtop, Version [1.0], http://sobereva.com/soft/Sobtop: 2022.
28. Q. Zha, Introduction to Electrode Process Kinetics, Beijing, China: Science Press 2002.
29. 30. D. C. Grahame, Chem. Rev., 1947, 41, 441.
30. W. Kohn & L. J. Sham. Self-consistent equations including exchange and correlation effects. Phys. Rev. 140, A1133-A1138 (1965).
31. A. Banerjee, N. Adams, J. Simons & R. Shepard. Search for stationary points on surfaces. J. Phys. Chem. 89, 52-57 (1985).

32. L. Martínez, Andrade R A , Birgin E G ,et al.PACKMOL: A package for building initial configurations for molecular dynamics simulations[J].Journal of Computational Chemistry, 2010, 30(13):2157-2164.

33. W. Humphrey, A. Dalke and K. Schulten, J. Mol. Graphics 1996, 14, 33.